PIER C

(Received 13 May 2025, Accepted 29 July 2025, Scheduled 5 August 2025)

Analysis of Vertically Polarized Plane Wave Scattering by Multi-Story Buildings with Windows

Cuong Manh Bui and Hiroshi Shirai*

Graduate School of Science and Engineering, Chuo University, Tokyo, Japan

ABSTRACT: An analysis of electromagnetic scattering by multi-story, multi-window buildings is presented by utilizing the Kirchhoff Approximation method. This investigation specifically analyzes scattering characteristics for vertically polarized incident plane waves. Scattering fields are calculated via radiation integrals associated with equivalent current sources induced on the building's exterior and across virtually closed window apertures by the incident wave. Fields within window regions are represented using rectangular waveguide modes, enabling the conversion of reflected fields from window glass into equivalent currents. The formulation's validity is established through comparisons with physical optics method and scale model measurements. Discussions address the influence of window glass and polarization on wave propagation in wireless communication scenarios like 4G LTE operating at 700 MHz.

1. INTRODUCTION

In urban environments, high-rise buildings often disrupt electromagnetic (EM) waves, shifting their paths and increasing multipath effects. Consequently, the analysis of high frequency scattering by multi-story buildings is crucial for designing reliable wireless networks with consistent coverage and low interference [1]. By examining how buildings scatter these waves, communication systems can be improved without relying on numerous field measurements or complex simulations.

For the accurate prediction of EM fields in urban environments, analysis of the scattering field by an individual building is essential. Calculating each building effectively allows for the study of more complex scenarios involving multiple structures. Research has demonstrated that building facades with glass windows have a significant impact on the scattered EM signal [2]. A comprehensive understanding of the building scattering can be achieved by the combination of scatterings by individual building walls and window apertures. In particular, due to high loss characteristics of wall materials at high frequencies, this behavior suggests that building walls may be treated as perfectly conducting surfaces.

The study of EM wave scattering by building windows can be approached using principles similar to those applied in analyzing EM diffraction by rectangular apertures in an infinitely large perfectly conducting plate. Several full-wave methods such as an eigenfunction expansion in terms of Mathieu functions [3] and Kobayashi Potential method [4] have addressed the calculation of the scattering field by windows. However, when aperture dimensions are large compared to the wavelength, these methods encounter numerical convergence problems and require significant amounts of memory and computational time.

To address convergence challenges, high-frequency asymptotic methods such as Geometrical Optics (GO), Geometrical Theory of Diffraction (GTD), Physical Optics (PO), and the Kirchhoff Approximation (KA) have been applied to analyze. In order to analyze involved scattering objects like a building with multiple windows, GO may be possible, but is computationally expensive as one has to trace all possible rays with multiple scattering effect such as reflection and transmission [5]. GTD method has shown relatively accurate results, even in scenarios involving small apertures, when the effects of multiple-edge diffraction are taken into account [6]. However, deriving appropriate coefficients for diffraction by corners or dielectric wedges poses significant challenges for GTD method.

If one wants to calculate the re-radiation field from window apertures, PO [7] or KA [8] would be suitable approach, as these re-radiation fields can be calculated by radiation from equivalent current sources. When the windows are set indented from building outer surface, it is bothersome to apply PO except for normal incident case, as the additional surface current at illuminated indent side-walls should be considered.

Previous studies have demonstrated that KA method is effective in calculating scattering fields by a single glass window [8] and by high-rise buildings specifically for horizontal polarization [9]. In continuation of the research presented in [9], which explored building scattering under horizontal polarization, this paper provides a scattering analysis focused on vertically polarized incident plane waves. Significantly expanding upon the scope of the previous work, this study not only shows polarization differences but also transitions from a small-scale building model to a configuration representative of realistic multi-story buildings with window glasses operating at practical wireless communication frequencies.

This paper is organized into three principal sections. Section 2 details the theoretical formulation. Section 3 presents and discusses the numerical results, encompassing validation against both scale model measurements and results from the PO

* Corresponding author: Hiroshi Shirai (shirai@m.ieice.org).

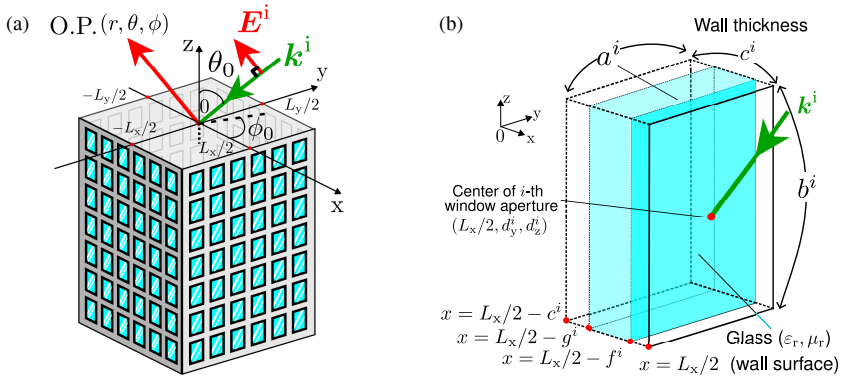

FIGURE 1. Configuration of the problem. (a) A high-rise building with multiple glass windows. (b) i-th window on the side-wall located at $x = L_x/2$.

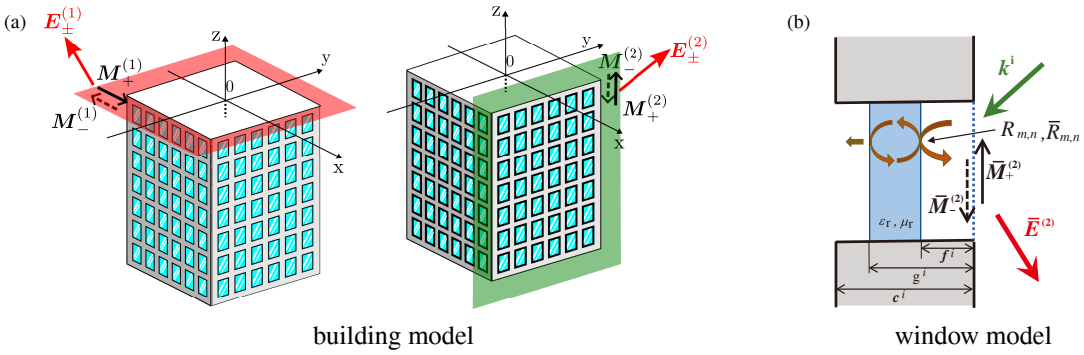

FIGURE 2. Analysis of scattering fields created by magnetic currents. (a) Scattering fields created by magnetic currents on the exterior of the roof ($z = 0$) and the side-wall ($x = L_x/2$). (b) Scattering field excited by magnetic currents on i-th window aperture on the building side-wall.

method obtained using Ansys High Frequency Structure Simulator Software (HFSS), and a detailed examination of the effects of windows, building size, and polarization. Finally, Section 4 provides general conclusions summarizing the key findings of this research.

2. FORMULATIONS

The scattering analysis focuses on a simplified building model illuminated by a vertically polarized plane wave, as shown in Fig. 1(a). The building, with dimensions L_x, L_y, L_z, consists of a flat roof and four side-walls positioned at $x = \pm L_x/2$ and $y = \pm L_y/2$. Each wall (thickness c^i) contains N glass windows. A detailed view of the i-th window on the wall at $x = L_x/2$ is provided in Fig. 1(b). This window has dimensions a^i (width) and b^i (height), and its center is located at $(d_x^i = L_x/2, d_y^i, d_z^i)$. The window aperture contains a glass slab characterized by relative permittivity ε_r, permeability μ_r, and thickness $g^i - f^i$. The outer surface of the glass is located at $x = L_x/2 - f^i$.

For the analysis of vertically polarized waves, the incident plane wave with the amplitude A_θ can be described with respect to the building roof by:

$$\boldsymbol{E}^{\mathrm{i}} = A_\theta \hat{\boldsymbol{\theta}}_0 e^{-j\boldsymbol{k}^{\mathrm{i}} \cdot \boldsymbol{r}}, \tag{1}$$

where '^' denotes the corresponding unit vector; $\boldsymbol{k}^{\mathrm{i}}$ and $\boldsymbol{r}$ represent the incident wave number vector and position vector to the observation point (O.P.), respectively. Recognizing that practical communication signals are often scattered and propagate in a near-horizontal region ($\theta_0 \sim \theta \sim \pi/2$), the numerical evaluations in this study are performed within the horizontal plane ($\theta_0 = \theta = \pi/2$.)

KA provides a methodology for determining the scattering field by the radiation from equivalent magnetic currents. These magnetic currents are induced on the building's exterior surfaces and on the surfaces of virtually closed window apertures, as shown in Fig. 2. Scattering from the building's outer edges is attributed to the fields $\boldsymbol{E}_{\pm}^{(1)}$, $\boldsymbol{E}_{\pm}^{(2)}$ excited by magnetic current sources $\boldsymbol{M}_{\pm}^{(1)}$, $\boldsymbol{M}_{\pm}^{(2)}$. Correspondingly, the window scattering field $\bar{\boldsymbol{E}}^{(2)}$, originates from the magnetic currents $\bar{\boldsymbol{M}}_{\pm}^{(2)}$ induced on the virtually closed window apertures. These currents $\bar{\boldsymbol{M}}_{\pm}^{(2)}$ are composed of currents from the incident plane wave and the reflection field at the glass layer within the window. The field inside each window can be analyzed using rectangular waveguide modes, allowing for theoretical calculation of the reflection field at the material layer via waveguide modal theory. The previous study provides detailed information on the field inside the window and its derivation [8]. When windows are spaced sufficiently far apart from each other and from the building edges, at distances exceeding the wavelength, the electromagnetic field interactions between them diminish significantly due to wave propagation effects and associated spatial decay. Consequently, these interactions can be neglected in the analysis. Therefore, the total scattering field by the building can be calculated by combining the individual scattering results

from the building edges and windows. Although conducting walls and window glasses produce scattered fields, re-radiation from the building's internal field is not considered in the subsequent analysis for simplicity.

2.1. Scattering Fields by the Outer Edges of the Building Roof and Side-Walls

Figure 2(a) illustrates the magnetic currents induced on the building roof's exterior. Using these currents, the far-field scattering field $\boldsymbol{E}_{\pm}^{(1)}$ is calculated via a vector potential approach, as derived in a previous work [9]:

$$E_r^{(1)} \sim 0, \tag{2}$$

$$E_\theta^{(1)} \sim -\mathrm{U}\Big(\frac{\pi}{2}-\theta_0\Big)\mathrm{sgn}\Big(\frac{\pi}{2}-\theta\Big)\frac{jA_\theta e^{-jkr}}{2\pi kr}k^2L_\mathrm{x}L_\mathrm{y} \cdot \mathrm{sinc}\Big(\frac{kL_\mathrm{x}\alpha}{2}\Big)\mathrm{sinc}\Big(\frac{kL_\mathrm{y}\beta}{2}\Big)\cos\theta_0\cos(\phi-\phi_0), \tag{3}$$

$$E_\phi^{(1)} \sim -\mathrm{U}\Big(\frac{\pi}{2}-\theta_0\Big)\mathrm{sgn}\Big(\frac{\pi}{2}-\theta\Big)\frac{jA_\theta e^{-jkr}}{2\pi kr}k^2L_\mathrm{x}L_\mathrm{y} \cdot \mathrm{sinc}\Big(\frac{kL_\mathrm{x}\alpha}{2}\Big)\mathrm{sinc}\Big(\frac{kL_\mathrm{y}\beta}{2}\Big)\cos\theta_0\cos\theta\sin(\phi_0-\phi), \tag{4}$$

where

$$\alpha = \sin\theta_0\cos\phi_0 + \sin\theta\cos\phi, \tag{5}$$

$$\beta = \sin\theta_0\sin\phi_0 + \sin\theta\sin\phi, \tag{6}$$

$$\gamma = \cos\theta_0 + \cos\theta, \tag{7}$$

and $\mathrm{U}(x)$ and $\mathrm{sgn}(x)$ are unit step and sign functions, respectively.

The scattering far-field $\boldsymbol{E}_{\pm}^{(2)}$ by the building side-wall at $x = L_\mathrm{x}/2$ can be derived analogously, considering it as radiation from equivalent magnetic current sources $\boldsymbol{M}_{+}^{(2)}$ on $x = L_\mathrm{x}/2_+$ and $\boldsymbol{M}_{-}^{(2)}$ on $x = L_\mathrm{x}/2_-$. The resulting fields $\boldsymbol{E}_{\pm}^{(2)}$ can then be combined as

$$E_r^{(2)} \sim 0, \tag{8}$$

$$E_\theta^{(2)} \sim -\left[\mathrm{U}\Big(\frac{\pi}{2}-\phi_0\Big)+\mathrm{U}\Big(\phi_0-\frac{3\pi}{2}\Big)\right] \cdot \mathrm{sgn}\Big(\phi-\frac{\pi}{2}\Big)\mathrm{sgn}\Big(\frac{3\pi}{2}-\phi\Big) \cdot \frac{jA_\theta e^{-jkr}}{2\pi kr}k^2L_\mathrm{y}L_\mathrm{z}e^{-j\gamma kL_\mathrm{z}/2}e^{j\alpha kL_\mathrm{x}/2} \cdot \mathrm{sinc}\Big(\frac{\gamma kL_\mathrm{z}}{2}\Big)\mathrm{sinc}\Big(\frac{\beta kL_\mathrm{y}}{2}\Big)\sin\theta_0\cos\phi, \tag{9}$$

$$E_\phi^{(2)} \sim \left[\mathrm{U}\Big(\frac{\pi}{2}-\phi_0\Big)+\mathrm{U}\Big(\phi_0-\frac{3\pi}{2}\Big)\right] \cdot \mathrm{sgn}\Big(\phi-\frac{\pi}{2}\Big)\mathrm{sgn}\Big(\frac{3\pi}{2}-\phi\Big) \cdot \frac{jA_\theta e^{-jkr}}{2\pi kr}k^2L_\mathrm{y}L_\mathrm{z}e^{-j\gamma kL_\mathrm{z}/2}e^{j\alpha kL_\mathrm{x}/2} \cdot \mathrm{sinc}\Big(\frac{\gamma kL_\mathrm{z}}{2}\Big)\mathrm{sinc}\Big(\frac{\beta kL_\mathrm{y}}{2}\Big) \cdot (\sin\theta_0\cos\theta\sin\phi - \cos\theta_0\sin\theta\sin\phi_0). \tag{10}$$

Unlike the previous analysis presented in [9], which focused solely on horizontal polarization of the incident wave, this work considers vertical polarization. This subtle change has a significant impact on the resulting scattering field. Specifically, vertical polarization introduces a non-zero theta component to $\boldsymbol{E}_{\pm}^{(2)}$. As noted, while TE and TM polarizations conveniently describe plane waves incident on a surface with a normal z-axis (horizontal), these definitions are no longer uniquely valid for describing the polarization state on surfaces with different orientations. Consequently, even though the roof is illuminated by a single polarization (TM, referred to here as vertical polarization), the vertical walls are illuminated by a superposition of both TE and TM field components. In the horizontally polarized case (TE on the roof) [9], the TE and TM components on the vertical wall cancel each other with respect to the theta component of the electric field. However, with vertical polarization (TM on the roof), this cancellation no longer occurs, leading to a non-zero theta component in $\boldsymbol{E}_{\pm}^{(2)}$. This inclusion is crucial for accurately predicting the far-field behavior of the building under vertically polarized illumination.

As the formulation for the scattered fields from the other side-walls can be derived in a similar manner, they are omitted here.

2.2. Scattering Fields by Building Windows

Window scattering can be modeled similarly to scattering by a hole in a thick conducting screen, where rectangular waveguide modes describe the fields within the aperture. Using the far-field scattering derivation for a single window in [8] and assuming negligible coupling between windows and building edges, the scattering field by N windows on the building wall at $x = L_\mathrm{x}/2$ is obtained by superposition.

Referring to the configuration shown in Fig. 2(b), modal reflection occurs at the glass layer interface $x = (L_\mathrm{x}/2 - f^i, L_\mathrm{x}/2 - g^i)$. This phenomenon is driven by the incidence of fields originating from the equivalent magnetic currents $\bar{\boldsymbol{M}}_{-}^{(2)}$. The reflection coefficients $R_{m,n}$ and $\bar{R}_{m,n}$ for TE_{mn} and TM_{mn} modes at this glass interface can be obtained by using modal waveguide theory that inherently accounts for multiple reflections within the glass layer:

$$R_{m,n} = \Big[e^{2jk'_{m,n}(f^i-g^i)}-1\Big]e^{-2jk_{m,n}f^i} \cdot \frac{(k'_{m,n})^2-(\mu_\mathrm{r}k_{m,n})^2}{\left\{\begin{array}{l}(\mu_\mathrm{r}k_{m,n}+k'_{m,n})^2 \\ -(\mu_\mathrm{r}k_{m,n}-k'_{m,n})^2e^{2jk'_{m,n}(f^i-g^i)}\end{array}\right\}}, \tag{11}$$

$$\bar{R}_{m,n} = \Big[e^{2jk'_{m,n}(f^i-g^i)}-1\Big]e^{-2jk_{m,n}f^i}$$

$$\cdot \frac{(k'_{m,n})^2 - (\varepsilon_{\mathrm{r}} k_{m,n})^2}{\left\{ \begin{array}{l} (\varepsilon_{\mathrm{r}} k_{m,n} + k'_{m,n})^2 \\ -(k'_{m,n} - \varepsilon_{\mathrm{r}} k_{m,n})^2 e^{2jk'_{m,n}(f^i - g^i)} \end{array} \right\}}, \quad (12)$$

where $k_{m,n}$ and $k'_{m,n}$ are the modal wave numbers outside and inside the glass layer as

$$k_{m,n} = k\sqrt{1 - (m\pi/ka^i)^2 - (n\pi/kb^i)^2}, \quad (13)$$

$$k'_{m,n} = k\sqrt{\varepsilon_{\mathrm{r}}\mu_{\mathrm{r}} - (m\pi/ka^i)^2 - (n\pi/kb^i)^2}. \quad (14)$$

The scattering field $\bar{\boldsymbol{E}}^{(2)}$ could be determined by summing the scattering contributions from each individual window as

$$\bar{E}_r^{(2)} \sim 0, \quad (15)$$

$$\begin{aligned} \bar{E}_\theta^{(2)} \sim{}& \left[\mathrm{U}\left(\frac{\pi}{2} - \phi_0\right) + \mathrm{U}\left(\phi_0 - \frac{3\pi}{2}\right)\right]\left[\mathrm{U}\left(\frac{\pi}{2} - \phi\right) + \mathrm{U}\left(\phi - \frac{3\pi}{2}\right)\right] \\ &\cdot \frac{jA_\theta e^{-jkr}}{2\pi kr} \sum_{i=1}^{N} e^{jk[\alpha(L_{\mathrm{x}}/2) + \beta d_{\mathrm{y}}^i + \gamma d_{\mathrm{z}}^i]} \\ &\cdot \left\{ -k^2 a^i b^i \mathrm{sinc}\left(\frac{ka^i\beta}{2}\right)\mathrm{sinc}\left(\frac{kb^i\gamma}{2}\right)\sin\theta_0\cos\phi \right. \\ &+ \sum_{m=0}^{\infty}\sum_{n=0}^{\infty} \frac{(k^2 a^i b^i)^2 B_{m,n}^{(2)} \cos\theta\cos\phi}{(m\pi/ka^i)^2 + (n\pi/kb^i)^2} \\ &\left. \cdot \left[\left(\frac{m\pi}{ka^i}\right)^2 R_{m,n}\bar{M}_{m,n}^{(2)} - \frac{mn\pi^2}{k^2 a^i b^i}\bar{R}_{m,n}\bar{N}_{m,n}^{(2)}\right] \right\}, \end{aligned} \quad (16)$$

$$\begin{aligned} \bar{E}_\phi^{(2)} \sim{}& \left[\mathrm{U}\left(\frac{\pi}{2} - \phi_0\right) + \mathrm{U}\left(\phi_0 - \frac{3\pi}{2}\right)\right]\left[\mathrm{U}\left(\frac{\pi}{2} - \phi\right) + \mathrm{U}\left(\phi - \frac{3\pi}{2}\right)\right] \\ &\cdot \frac{jA_\theta e^{-jkr}}{2\pi kr} \sum_{i=1}^{N} e^{jk[\alpha(L_{\mathrm{x}}/2) + \beta d_{\mathrm{y}}^i + \gamma d_{\mathrm{z}}^i]} \\ &\cdot \left\{ -k^2 a^i b^i \mathrm{sinc}\left(\frac{ka^i\beta}{2}\right)\mathrm{sinc}\left(\frac{kb^i\gamma}{2}\right) \right. \\ &\cdot (\cos\theta_0 \sin\theta \sin\phi_0 - \sin\theta_0 \cos\theta \sin\phi) \\ &+ \sum_{m=0}^{\infty}\sum_{n=0}^{\infty} \frac{(k^2 a^i b^i)^2 B_{m,n}^{(2)} \sin\phi}{(m\pi/ka^i)^2 + (n\pi/kb^i)^2} \\ &\cdot \left[R_{m,n}\bar{M}_{m,n}^{(2)} \left[\left(\frac{n\pi}{kb^i}\right)^2 \sin^2\theta - \left(\frac{m\pi}{ka^i}\right)^2 \cos^2\theta\right] \right. \\ &\left. \left. + \frac{mn\pi^2}{k^2 a^i b^i}\bar{R}_{m,n}\bar{N}_{m,n}^{(2)} \right] \right\}, \end{aligned} \quad (17)$$

where

$$B_{m,n}^{(2)} = \frac{(-1)^{m+1} e^{j(ka^i/2)\sin\theta\sin\phi} + e^{-j(ka^i/2)\sin\theta\sin\phi}}{(m\pi)^2 - (ka^i\sin\theta\sin\phi)^2}$$

$$\cdot \frac{(-1)^{n+1} e^{j(kb^i/2)\cos\theta} + e^{-j(kb^i/2)\cos\theta}}{(n\pi)^2 - (kb^i\cos\theta)^2}, \quad (18)$$

$$\bar{M}_{m,n}^{(2)} = \frac{\pi^2 \epsilon_m \epsilon_n}{2k^2 a^i b^i}\bar{B}_{m,n}^{(2)}\left[\left(mkb^i\right)^2 + \left(nka^i\sin\phi_0\right)^2\right]\sin(2\theta_0), \quad (19)$$

$$\bar{N}_{m,n}^{(2)} = 2mn\pi^2 \bar{B}_{m,n}^{(2)} \sin(2\theta_0)\cos^2(\phi_0), \quad (20)$$

$$\bar{B}_{m,n}^{(2)} = \frac{(-1)^{m+1} e^{j(ka^i/2)\sin\theta_0\sin\phi_0} + e^{-j(ka^i/2)\sin\theta_0\sin\phi_0}}{(m\pi)^2 - (ka^i\sin\theta_0\sin\phi_0)^2}$$

$$\cdot \frac{(-1)^{n+1} e^{j(kb^i/2)\cos\theta_0} + e^{-j(kb^i/2)\cos\theta_0}}{(n\pi)^2 - (kb^i\cos\theta_0)^2}, \quad (21)$$

and

$$\epsilon_j = \begin{cases} 1 & (j = 0) \\ 2 & (j > 0). \end{cases} \quad (22)$$

The derived KA formulas do not include a parameter for wall thickness c^i because it primarily affects the internal scattering field and not the external field as discussed in the previous works [8, 9].

3. NUMERICAL RESULTS AND DISCUSSION

The numerical validation discussion starts by defining the specific computational settings. All far-field scattering patterns have been normalized by factor $jA_\theta e^{-jkr}/(2\pi r)$. To accurately model the window and glass effects, the infinite waveguide mode series were truncated to retain the propagating and the first three evanescent modes [10]. Furthermore, multiple internal reflections and transmissions within the glass material are accounted for via the reflection coefficients defined in Eqs. (11) and (12). It is important to note that the derived formulations remain valid for arbitrary window configurations as long as adjacent apertures are electrically well separated.

3.1. Comparison with Measurement and Other Method

Let us explain about measurement setup of scale models for comparison. The first model represents a building without windows, whereas the second model includes 64 windows. Both models possess identical external dimensions ($L_{\mathrm{x}} = 28\,\mathrm{cm}$, $L_{\mathrm{y}} = 28\,\mathrm{cm}$, $L_{\mathrm{z}} = 32\,\mathrm{cm}$). The model presented in Fig. 3 features a building, whose each side-wall contains 4×4 glassless windows. The window dimensions are $a^i = 4\,\mathrm{cm}$, $b^i = 5.5\,\mathrm{cm}$, and the window apertures on each wall are evenly distributed. Bi-static scattering measurements have been performed at 5.9 GHz in an anechoic chamber room as depicted in Fig. 4 [9]. Because of the tight chamber space, both the transmitting (Tx) and receiving (Rx) antennas are positioned 4.5 m away from the building model with the bistatic angle of 45°. Then the far-field condition has been satisfied.

Figure 5 presents the bistatic scattering patterns for E_θ in the horizontal plane ($\theta_0 = \theta = \pi/2$). Results obtained using the KA method are compared with both experimental measurements (normalized to peak amplitude) and simulations em-

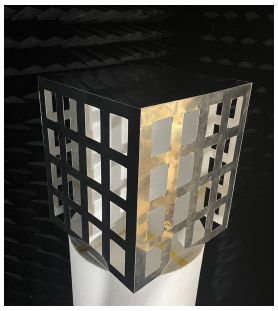

FIGURE 3. A scale building models with 64 glassless windows for measurement. $L_x = L_y = 28$ cm, $L_z = 32$ cm.

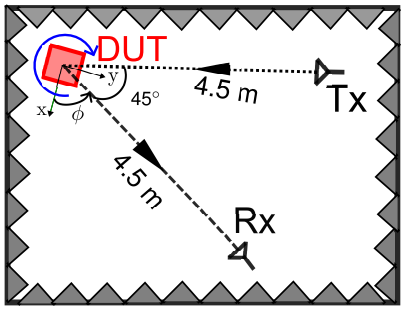

FIGURE 4. Top view of the bistatic measurement setup in an anechoic chamber room.

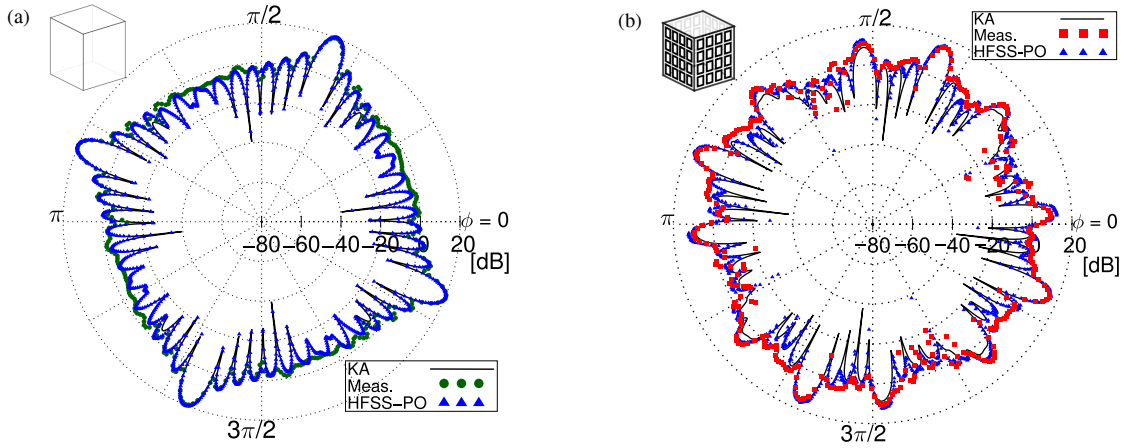

FIGURE 5. Comparison of the bistatic scattering pattern E_θ between buildings with and without glassless windows. $f = 5.9$ GHz. $\theta_0 = \theta = \pi/2$. $\phi_0 = \phi + \pi/4$. $L_x = L_y = 28$ cm, $L_z = 32$ cm. (a) Without window. (b) With glassless windows.

ploying the PO method in Ansys HFSS. Good agreement is observed among the KA results, PO simulations, and measurement data, particularly in reproducing the four distinct main lobes generated by specular reflections from the building's side-walls.

It is noted that the computation time for our KA method is only 0.12 seconds for Fig. 5(b), with 7136 seconds for HFSS-PO. Potential sources of minor differences include fabrication tolerances of the building models, coupling effects between the window apertures, and re-radiation from internal structures. For the glassless window configuration, the pattern exhibits characteristic minor lobes consistent with grating effects shown in Fig. 5(b), which can be predicted using the grating theory as discussed in [9]. Radiation at the apertures is made only by aperture rim and no re-radiation contribution due to waveguide modal reflection at glass layer. Accordingly, PO solution is pretty accurate. It is noted that under the $\theta = \theta_0 = \pi/2$ condition, the roof's contribution to the overall scattering vanishes. This is because the scattered field components $E_\theta^{(1)}$ and $E_\phi^{(1)}$, as defined in Eqs. (3) and (4), are dependent on $\cos\theta_0$ and $\cos\theta$ factors which become zero in this case.

3.2. Numerical simulation for 700 MHz

Having validated our formulation with the other methods, we now utilize standard bistatic patterns with ($\theta_0 = \theta = \pi/2$) and ($\phi_0 = \pi/4$) to present the KA results for a thorough examination of scattering behavior in urban settings relevant to 4G LTE mobile communications. The operating frequency is set at 700 MHz. All building models share the same dimensions: $L_x = L_y = 17.1$ m (39.98λ) and $L_z = 22.9$ m (53.41λ). Each building incorporates 168 windows ($6 \times 7 \times 4$) distributed uniformly across all walls. Each window has dimensions of $a^i = 1.7$ m (3.97λ) and $b^i = 2.3$ m (5.37λ). Soda-silica glass, characterized by a relative permittivity of $\varepsilon_r = 7.2 - j0.15$ and relative permeability $\mu_r = 1$ [11], is positioned at the window top ($f^i = 0$). The glass thickness is 1.5 cm.

Figure 6 shows patterns of the scattered far field by three building models. Three types of buildings are examined: one without windows, one with glassless windows, and one with glass windows. The scattering pattern of such an electrically large building becomes highly oscillatory due to the interference between scattering components. Two strong reflections are visible at specular angles ($\phi = 3\pi/4, 7\pi/4$). They are caused by the building's side-walls at $y = L_y/2$ and $x = L_x/2$. A forward scattering peak is also presented at ($\phi = 5\pi/4$). The patterns for all three buildings exhibit similarity when ϕ is between π and $3\pi/2$. This is attributed to the sides of the building at $x = -L_x/2$ and $y = -L_y/2$ being in the shadow region. Thus, in this region, the scattering primarily arises from the edges of the building faces at $x = L_x/2$ and $y = L_y/2$. In

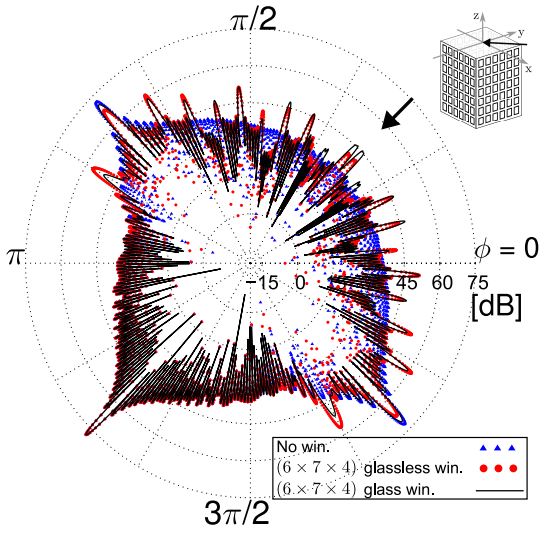

FIGURE 6. Bistatic scattering pattern E_θ comparison among three 7-story buildings: no window, 168 $(6 \times 7 \times 4)$ windows with/without glass. $f = 700\,\text{MHz}$. $\theta_0 = \theta = \pi/2$. $\phi_0 = \pi/4$. $L_\text{x} = L_\text{y} = 17.1\,\text{m}$, $L_\text{z} = 22.9\,\text{m}$. Dimension of each window is $a^i = 1.7\,\text{m}$, $b^i = 2.3\,\text{m}$. Dielectric glasses ($\varepsilon_\text{r} = 7.20 - j0.15$) are set at the top of each window ($f^i = 0$). The glass thickness ($g^i - f^i$) is 1.5 cm.

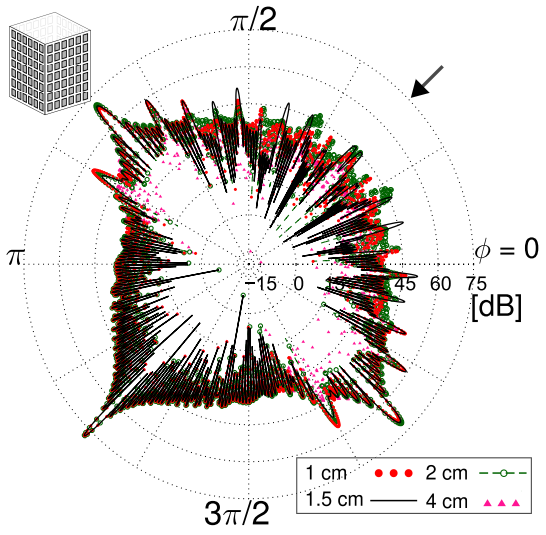

FIGURE 7. Bistatic scattering pattern E_θ comparison among buildings with 168 $(6 \times 7 \times 4)$ windows when the thickness of glass is changed: 1.0, 1.5, 2.0, and 4.0 cm. Other parameters are the same as in Fig. 6.

the illuminated areas ($0 < \theta < \pi, 3\pi/2 < \theta < 2\pi$), extra peaks are also observed for two models with windows. These grating peaks may be created by the regular arrangement of windows on the building walls. Furthermore, due to the lossy material of glass, potential contributions to the signal at the side lobe peaks exist. Calculating the scattering by the building with glass window requires approximately 10 minutes using the KA method for 7200 points (measured every 0.05° for a full circle), while for the building without glass, it only takes 3.9 seconds.

Analyzing the impact of glass thickness provides valuable observations. Fig. 7 shows the scattering patterns for different

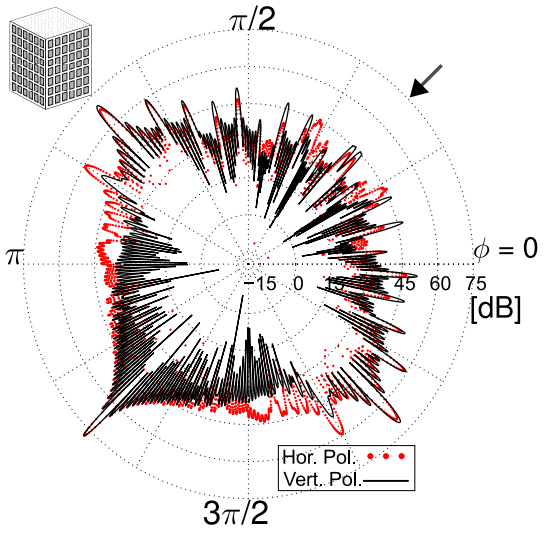

FIGURE 8. Comparison of the vertically polarized scattering field E_θ and the horizontally polarized scattering field E_ϕ by the building with glass windows. All parameters are the same as in Fig. 6.

thicknesses of glass. For all these thicknesses, glass thickness primarily affects the grating lobes and side lobes in the region $0 < \phi < \pi/2$. The main lobes, however, exhibit very little change. These effects arise from variations in the modal reflection coefficients with changing glass thickness [8]. Compared to the glassless scenario shown in Fig. 6, if detailed accuracy is not critical, the glassless model can significantly reduce calculation time.

Figure 8 shows the scattering far fields for the horizontally polarized scattering wave E_ϕ and vertically polarized scattering wave E_θ. Although the intensities of the scattering fields in the main beam directions are similar, there are some differences in the grating and side lobes.

Figure 9 illustrates the effect of building face size by doubling the dimensions ($L_\text{x} = 34.2\,\text{m}$) of the face at $y = \pm L_\text{y}/2$. Examining the angular range of $\pi/2 < \phi < \pi$ shows a clear effect of this size increase: the reflection lobe peak at $\phi = 3\pi/4$ becomes larger, accompanied by a noticeable rise in the number of minor lobes and the appearance of sharper diffraction lobes. These observations can be explained mathematically by the $\text{sinc}(\alpha k L_\text{x}/2)$ term in Eq. (9). Maintaining a constant number of windows while adjusting their distribution leads to a change of multiple grating lobes. In contrast to earlier findings where scattering remained consistent in the $\pi < \phi < 3\pi/2$ region, the current scenario exhibits an increase in the strength of main lobes at $\phi = 5\pi/4$. However, the scattering characteristic in the $3\pi/2 < \phi < 2\pi$ region remains mostly unchanged, primarily because the scattering is dominated by the unchanging building face at $x = L_\text{x}/2$, while the modified face at $y = L_\text{y}/2$ contributes minimally in this angular range.

Finally, Fig. 10 shows the scattering patterns for two multi-story buildings: one with seven stories ($L_\text{z} = 22.9\,\text{m}$) and the other with four stories ($L_\text{z} = 13.4\,\text{m}$). Although the overall shapes of the scattering pattern are similar in the two cases, the intensities differ. This difference mainly stems from the smaller effective scattering cross section associated with the lower L_z.

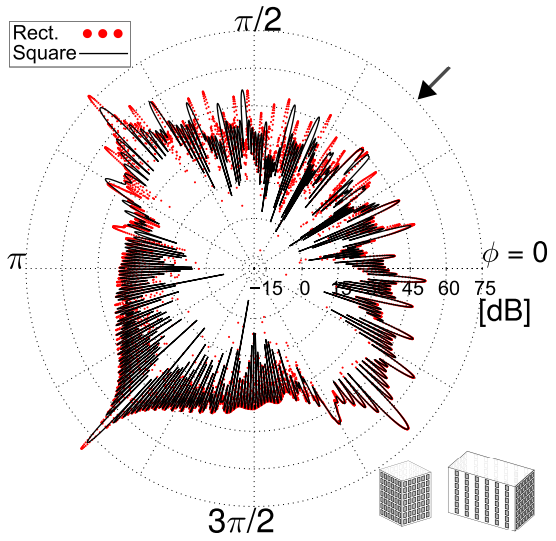

FIGURE 9. Bistatic scattering pattern E_θ comparison when dimension of building changes. All parameters are the same as in Fig. 6 for the building with glass windows, except $L_x = 34.2\,\text{m}$ for the larger rectangular building.

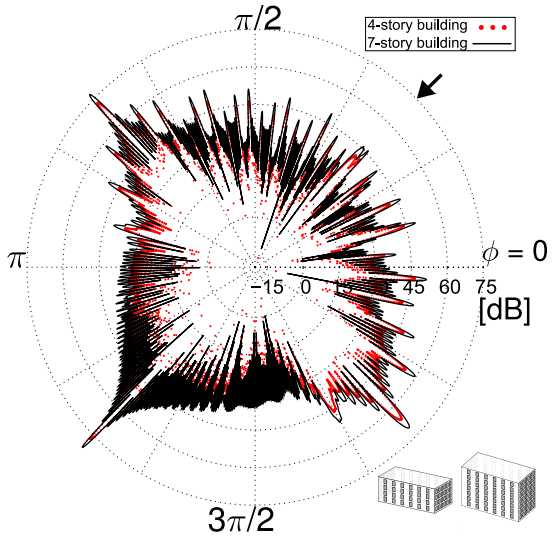

FIGURE 10. Bistatic scattering pattern E_θ between building with $6 \times 7 \times 4$ glass windows (7-story building, $L_z = 22.9\,\text{m}$) and $6 \times 4 \times 4$ glass windows (4-story building $L_z = 13.4\,\text{m}$). All parameters are the same as in Fig. 9.

4. CONCLUSION

This research has presented a high-frequency analysis based on the KA method to characterize vertically polarized scattering by multi-story buildings. The analysis demonstrates that for sufficiently spaced windows and building edges (separation greater than the wavelength), the total scattering field might be approximated by summing contributions from equivalent magnetic currents. These currents are induced on the virtually closed window apertures and building's exterior, and their excitation accounts for both the incident wave and waveguide mode reflections from window glass.

The validity of the proposed KA method has been rigorously verified through comparisons with scale model measurements and PO simulations, demonstrating a good level of accuracy. Furthermore, the analysis has provided valuable insights into the scattering impacts of window, glass, polarization, and building height in terms of number of stories.

Future research will be directed toward expanding analytical capabilities to include the near-field region. This advancement is motivated by the pressing need for detailed EM environment maps, which are essential for the strategic planning and deployment of next-generation urban radio communication networks.

ACKNOWLEDGEMENT

A part of this work has been supported by a Scientific Research Grant In Aide (23K03860, 2023) from the Japan Society for the Promotion of Science, Japan, and 2024 Chuo University Grant for Special Research.

REFERENCES

[1] Bertoni, H. L., *Radio Propagation For Modern Wireless Systems*, Pearson Education, 1999.

[2] Lu, J. S., H. L. Bertoni, and V. Degli-Esposti, "Scale model investigation of mechanisms for scattering from office buildings at 2 GHz," *IEEE Transactions on Antennas and Propagation*, Vol. 62, No. 12, 6435–6442, Dec. 2014.

[3] Morse, P. M. and P. J. Rubenstein, "The diffraction of waves by ribbons and by slits," *Physical Review*, Vol. 54, No. 11, 895, Dec. 1938.

[4] Serizawa, H., "Diffraction by a rectangular hole in a thick conducting screen," *Novel Imaging and Spectroscopy*, 79–100, 2019.

[5] Pongsilamanee, P. and H. L. Bertoni, "Specular and nonspecular scattering from building facades," *IEEE Transactions on Antennas and Propagation*, Vol. 52, No. 7, 1879–1889, Jul. 2004.

[6] Shimizu, M., H. Shirai, and R. Sato, "Electromagnetic scattering analysis by a window model on a building wall," *IEICE Trans. Electron.*, Vol. J100-C, 295–301, Jul. 2017.

[7] Diaz, L. and T. Milligam, *Antenna Engineering Using Physical Optics*, Artech House, Norwood, MA, USA, 1996.

[8] Bui, C. M., K. N. Nguyen, and H. Shirai, "Electromagnetic wave scattering analysis by a window aperture on a conducting wall," *Progress In Electromagnetics Research C*, Vol. 122, 95–108, 2022.

[9] Bui, C. M. and H. Shirai, "High frequency plane wave scattering analysis by large buildings with multiple windows," *IEICE Transactions on Electronics*, Vol. E108-C, 179–188, 2025.

[10] Nguyen, K. N. and H. Shirai, "Kirchhoff approximation analysis of plane wave scattering by conducting thick slits," *IEICE Transactions on Electronics*, Vol. 102, No. 1, 12–20, Jan. 2019.

[11] Hippel, A. R. V., *Dielectric Materials and Applications*, MIT Press, New York, 1954.